Environmental Pollution 262 (2020) 114356

Contents lists available at ScienceDirect

Environmental Pollution

journal homepage: www.elsevier.com/locate/envpol

Isotopic tracing of mercury sources in estuarine-inner shelf sediments of the East China Sea☆

Xiang Sun [a, b], Runsheng Yin [c, d], Limin Hu [b, e], Zhigang Guo [a, b, *], James P. Hurley [f, g], Ryan F. Lepak [f], Xiangdong Li [d]

[a] Department of Environmental Science and Engineering, Fudan University, Shanghai 200438, China
[b] Laboratory for Marine Geology, Qingdao National Laboratory for Marine Science and Technology, Qingdao 266061, China
[c] State Key Laboratory of Ore Deposit Geochemistry, Institute of Geochemistry, Chinese Academy of Sciences, Guiyang 550081, China
[d] Department of Civil and Environmental Engineering, The Hong Kong Polytechnic University, Hung Hom, Kowloon, Hong Kong
[e] Key Laboratory of Marine Sedimentology and Environmental Geology, First Institute of Oceanography, Ministry of Natural Resources, Qingdao 266061, China
[f] Environmental Chemistry and Technology Program, University of Wisconsin-Madison, Madison, WI, 53706, USA
[g] Department of Civil and Environmental Engineering, University of Wisconsin-Madison, Madison, WI, 53706, USA

ARTICLE INFO

Article history:
Received 27 December 2019
Received in revised form
16 February 2020
Accepted 9 March 2020
Available online 12 March 2020

Keywords:
Burial flux
Estuarine-inner shelf system
Isotopic tracing
Mercury
Quantitative source apportionment

ABSTRACT

Large river estuarine-inner shelf systems play an important role in the coastal biogeochemical cycling of heavy metals; however, the source-to-sink of mercury (Hg) in these environments remain poorly understood. In this study, the Hg isotopic composition of surface sediments in the Yangtze River Estuary (YRE) and inner shelf of the East China Sea (ECS) were examined to quantitatively track Hg sources in this region. We detected large spatial variation in δ^{202}Hg (−1.88 to −0.29‰) and Δ^{199}Hg (−0.22 to 0.13‰) in sediments of the YRE-ECS inner shelf. The impact of sediment resuspension and transport from the YRE to the inner shelf of the ECS could have little effect on Hg isotopic composition, and the two regions shared similar Hg isotopic composition. An isotope-based triple mixing model further revealed major contributors to sediment Hg from industrial Hg discharge into water (51.8 ± 24.5%), soil Hg from surface runoff (29.2 ± 17.0%), and precipitation-derived atmospheric deposition Hg (19.1 ± 17.5%). The Hg isotopic compositions of the YRE sediments and other local river estuaries were similar to those of direct industrial Hg discharge, indicating that contaminated riverine discharge was the dominant Hg source for estuarine and adjacent shelf areas. Soil Hg delivered through surface runoff was the primary source of Hg to the coastal areas not near large river estuaries, whereas precipitation-derived atmospheric deposition had a greater influence on offshore sediment Hg content. Industrial Hg discharged to rivers had the highest mean depositional flux (35.0 ± 27.3 ng cm^{-2} yr^{-1}) and mass inventory (25.6 t yr^{-1}), accounting for 77.4% of the total Hg variance. The findings of this study demonstrate that large rivers such as the Yangtze River can supply substantial amounts of industrial Hg to the estuary and adjacent shelf.

1. Introduction

Mercury (Hg) is a semi-volatile heavy metal that is released to the environment from natural and anthropogenic activity (Martinez-Cortizas et al., 1999; Mason and Sheu, 2002; Sun et al., 2019) and can be rapidly transported within the atmosphere. Anthropogenic emissions contribute about 2.5 kiloton (kt) Hg to the atmosphere every year, increasing atmospheric Hg concentrations by about 450% above levels before 1450 AD (Outridge et al., 2018). About 3.8 kt Hg per year is deposited from the atmosphere to oceans (Outridge et al., 2018); marine environments also receive about 0.3 kt Hg from rivers (Driscoll et al., 2013; Outridge et al., 2018). In aquatic ecosystems, Hg^{2+} can be converted into methylmercury (MeHg), a bioavailable neurotoxin that can jeopardize human health through biomagnification in the food chain (Mahaffey et al., 2011).

Recent studies have improved our understanding of the biogeochemical cycle of Hg by exploring isotopic Hg compositions

☆ This paper has been recommended for acceptance by Philip Smith.

* Corresponding author. Department of Environmental Science and Engineering, Fudan University, Shanghai 200438, China.
E-mail address: guozgg@fudan.edu.cn (Z. Guo).

https://doi.org/10.1016/j.envpol.2020.114356
0269-7491/

in nature. Hg has seven stable isotopes (^{196}Hg, ^{198}Hg, ^{199}Hg, ^{200}Hg, ^{201}Hg, ^{202}Hg, and ^{204}Hg), with a 4% difference in relative mass (Blum and Bergquist, 2007). Biogeochemical processes trigger mass-dependent fractionation (MDF, usually reported as δ^{202}Hg) and mass-independent fractionation (MIF, usually reported as Δ^{199}Hg) of Hg isotopes (Bergquist and Blum, 2007; Blum et al., 2014). Large variation (>10‰) in both δ^{202}Hg and Δ^{199}Hg values has been reported in the main Hg reservoirs on Earth (Blum et al., 2014), suggesting that Hg isotopes can be used to identify Hg sources or monitor key environmental processes.

Coastal areas are interfaces of land and marine ecosystems that exhibit complex biogeochemical processes, especially in large river estuaries that receive huge amounts of pollutants from the watershed (Bianchi and Allison, 2009). The East China Sea (ECS) is a marginal sea greatly influenced by the Yangtze River, which is the fifth largest river in the world in terms of water discharge and the fourth largest in terms of sediment discharge (Wang et al., 2011). The drainage basin of the Yangtze River covers an area of 1.94×10^6 km^2, representing about 20% of the Chinese mainland. The Yangtze River Delta Economic Belt is among the most industrialized and urbanized regions in China, accounting for >40% of the national gross domestic product (Yang et al., 2006a,b). The Yangtze River discharged about 60 Mg Hg to the ECS in 2006 (Liu et al., 2016), greatly impacting its biogeochemical processes; while Qiantang River discharged 4.4 Mg Hg in 2004 (Su et al., 2011) and Min River discharged 8.7 Mg Hg in 2008 (Du et al., 2013).

Several recent studies have investigated Hg isotopic composition in surface sediments from Chinese marginal seas (Yin et al., 2015; Yin et al., 2018; Zhang et al., 2018; Meng et al., 2019). Dramatic differences in δ^{202}Hg (−2.82 to −0.09‰) and Δ^{199}Hg (−0.15 to 0.45‰) have been reported in Chinese marginal sea sediments, suggesting a mixture of Hg derived from industrial, soil, and precipitation sources in varying proportions depending on location. Hg contributions from these three sources have been quantified using isotope-based triple-mixing models (Yin et al., 2015; Yin et al., 2018; Meng et al., 2019). However, our recent study demonstrated that Hg depositional flux varied widely in sediments from the Yangtze River Estuary (YRE) and inner shelf of the ECS, highlighting the importance of riverine input to Hg source-sink processes and regional budgets (Liu et al., 2017). Ocean currents and tidal currents in the region redistribute sediments trapped in muddy areas (Milliman et al., 1985; Guo et al., 2006; Li et al., 2017); therefore, a combination of depositional flux, Hg isotope, and source apportionment data may offer greater insight into Hg biogeochemical cycling in this complex region. In this study, we explored isotopic compositions of Hg in YRE-ECS inner shelf sediments, to refine Hg source apportionment estimates using a previously established isotope-based triple-mixing model (Yin et al., 2015; Yin et al., 2018). We then combined the model output with our previous depositional Hg flux results (Liu et al., 2017) to further estimate the depositional flux of the industrial, soil, and precipitation Hg sources in the region.

2. Material and methods

2.1. Study area

The YRE adjoins the inner-shelf of ECS, which is located in the east of China and the west of the Pacific Ocean. After passing through the Three Gorges Dam, the Yangtze River discharges about 1.36×10^8 tons of sediments into the ECS annually (Yang et al., 2006a,b; Yang et al., 2018); most of them are trapped as the YRE mud and Zhejiang-Fujian Coastal mud due to the net effect of ocean currents (Fig. 1) (Milliman et al., 1985; Liu et al., 2006). The Yangtze River discharges about 87% of its annual sediment in the flood season (June–October), when the Zhejiang-Fujian coastal current is weak and the Taiwan Warm Current is strong due to the prevailing southeast monsoon (Guo et al., 2007). This fluvial hydrodynamic setting leads to the accumulation of Yangtze-derived sediments in the subaqueous delta and estuarine system, forming the YRE mud (Liu et al., 2007; Liu et al., 2006). In winter, driven by the northwesterly East Asian monsoon, strong northwesterly wind-induced waves readily resuspend the newly deposited sediments, which are then transported along the inner shelf by the southward Zhejiang-Fujian coastal current. These materials are constrained to the inner shelf of the ECS by obstruction of the strong northward-flowing Taiwan Warm Current, thus forming the Zhejiang-Fujian Coastal mud (Liu et al., 2007; Liu et al., 2006). Atmospheric particles and associated pollutants derived from Asian dust are also deposited into the ECS in spring and winter annually (Guo et al., 2006).

2.2. Sampling

During two campaigns, we collected 70 surface sediment samples (0–3 cm) from the YRE (E sites) and ECS inner shelf (S sites) using a stainless steel box core (Fig. 1). We sampled from sites E1, E3-E23, S1, S3–S5, and S8–S11 in June 2006 onboard the *R/V Dong Fang Hong 2* of the Ocean University of China, and from sites S12–S20 and S22–S52 in August 2007 onboard the *R/V Kan 407*. All samples were packed in aluminum foil, immediately refrigerated at −20 °C, and transported to the laboratory, where they were freeze-dried at −50 °C for 72 h and then ground and homogenized using a mortar and pestle before analysis. The sampling sites are described in Table S1. Concentrations of Hg and total organic carbon (TOC) and the median diameter (MD) of these sediment samples were previously reported (Liu et al., 2017), and their correlations and distributions are shown in Figs. S1 and S2, respectively.

2.3. Hg isotopic composition analysis

Hg isotopic compositions were analyzed at the University of Wisconsin, Madison, State Laboratory of Hygiene. About 0.5 g of each sample was digested (95 °C, 1 h) in 5 mL *aqua regia* (HCl/HNO_3 = 3, *v*/*v*). Milli-Q water was used to dilute each digested sample to 0.5 ng mL^{-1} Hg and <20% acid. Hg concentrations and acid matrix were matched between the diluted sample and a bracketing standard (NIST SRM 3133, in 15% *aqua regia*). Hg isotopic composition was measured using Neptune Plus multicollector inductively coupled plasma mass spectrometry (MC-ICP-MS) system following a previously described method (Yin et al., 2016a,b,c). Hg concentrations were too low for isotopic analysis at sites S4, S11, E4-E5, E11, and E18-E22 (almost all offshore sampling sites); these samples were therefore omitted from subsequent analysis. The samples were bracketed with NIST SRM 3133 and Hg concentration and acid matrix. MDF were matched and reported as δ^{202}Hg (‰) as follows (Blum and Bergquist, 2007):

$$\delta^{202}\mathrm{Hg} = \left[\left(^{202}Hg/^{198}Hg\right)_{sample} \Big/ \left(^{202}Hg/^{198}Hg\right)_{\mathrm{SRM3133}}\right] - 1 \quad (1)$$

The difference between the measured δ^{xxx}Hg value and that predicted based on MDF and δ^{202}Hg is MIF, which is reported as Δ^{199}Hg, Δ^{200}Hg, and Δ^{201}Hg (‰) and calculated using the following equations (Blum and Bergquist, 2007):

$$\begin{aligned} \Delta^{199}Hg &\approx \delta^{199}Hg - (\delta^{202}Hg \times 0.2520) \\ \Delta^{200}Hg &\approx \delta^{200}Hg - (\delta^{202}Hg \times 0.5024) \\ \Delta^{201}Hg &\approx \delta^{201}Hg - (\delta^{202}Hg \times 0.7520). \end{aligned} \quad (2)$$

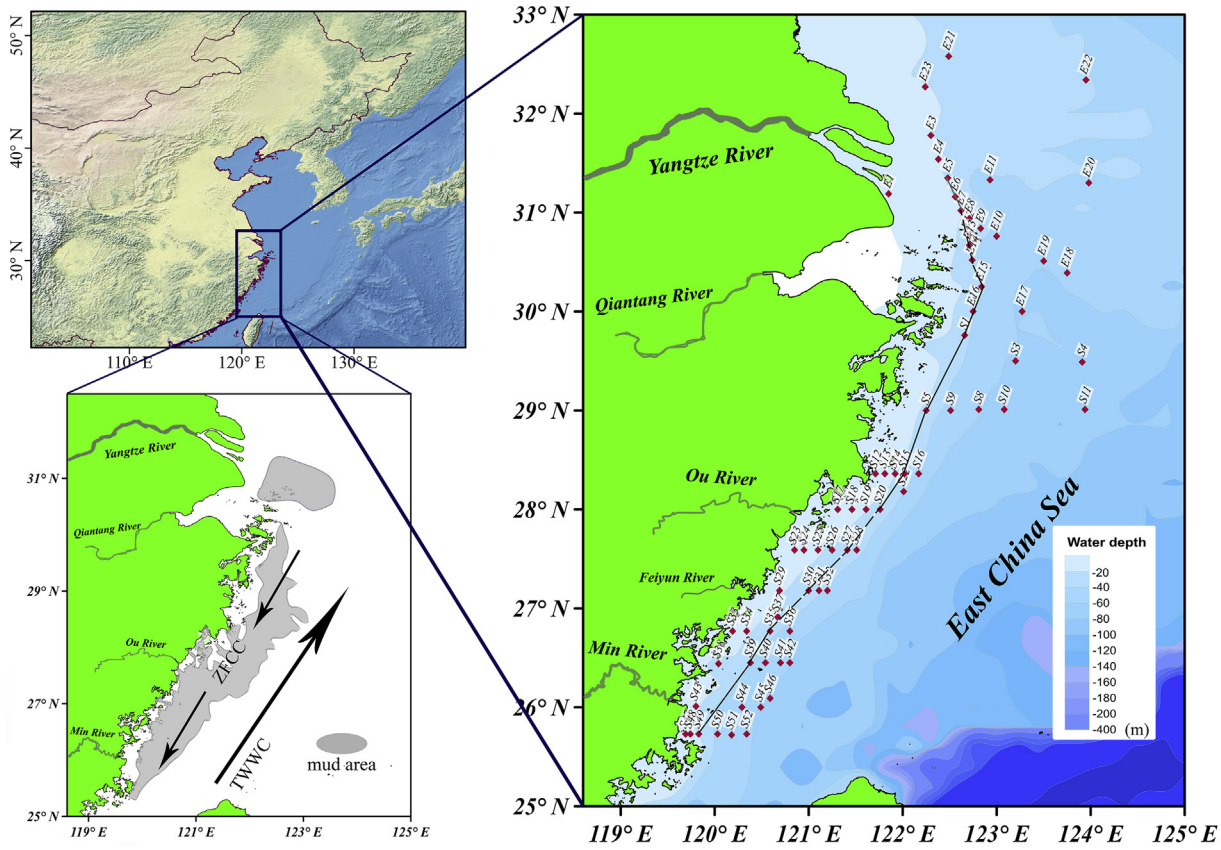

Fig. 1. Study area and sampling sites. TWWC: Taiwan Warm Current; ZFCC: Zhejiang-Fujian Coastal Current. Black line: north-south transect).

We measured UM-Almaden secondary Hg standard solution and a standard reference material, MESS-1, in the same manner as the samples. The isotopic compositions of UM-Almadén (δ^{202}Hg, −0.53 ± 0.09‰; Δ^{199}Hg, −0.04 ± 0.05‰; Δ^{200}Hg, 0.00 ± 0.04‰; Δ^{201}Hg, 0.00 ± 0.04‰; 2σ; n = 27) and MESS-1 (δ^{202}Hg, −1.89 ± 0.11‰; Δ^{199}Hg, −0.06 ± 0.01‰; Δ^{200}Hg, 0.07 ± 0.03‰; Δ^{201}Hg, −0.05 ± 0.03‰; 2σ; n = 4) (Table S3) agreed well with those reported previously (Blum and Bergquist, 2007; Yin et al., 2016a,b,c). The uncertainties detected in this study corresponded to values > 2 SD of either UM-Almadén or MESS-1.

3. Results and discussion

3.1. Hg isotopic compositions

According to our previous study of YRE-ECS inner shelf sediments (Liu et al., 2017), Hg concentrations were characterized by a decreasing Hg gradient with increasing distance from mainland China (mean 46.3 ± 17.3 ng g^{-1}; 1σ; n = 70, Table S1). In the present study, we observed large variation in Hg isotopic compositions, with δ^{202}Hg ranging from −1.88 to −0.29‰ (mean, −1.03 ± 0.05‰; 1σ; n = 60), Δ^{199}Hg values from −0.22 to 0.13‰ (mean, −0.03 ± 0.02‰; 1σ; n = 60), and Δ^{200}Hg values from −0.10 to 0.10‰ (mean, 0.00 ± 0.04‰; 1σ; n = 60) (Table S2).

The Δ^{199}Hg/Δ^{201}Hg ratio is a useful tool for examining the mechanism of Hg-MIF, as an indicator of the nuclear volume effect (NVE) (Schauble, 2007) and the magnetic isotope effect (MIE) (Buchachenko et al., 2007). A Δ^{199}Hg/Δ^{201}Hg ratio of 1.6–2.0 indicates NVE, which occurs during elemental Hg evaporation (Estrade et al., 2009; Ghosh et al., 2013) and equilibrium Hg-thiol complexation (Wiederhold et al., 2010). In contrast, a Δ^{199}Hg/Δ^{201}Hg ratio of 1.0–1.3 indicates MIE, which occurs during MeHg photodegradation (Bergquist and Blum, 2007) and aqueous Hg^{2+} photoreduction (Bergquist and Blum, 2007; Zheng and Hintelmann, 2009; Zheng and Hintelmann, 2010). The slope of Δ^{199}Hg/Δ^{201}Hg in this study was 0.96 ± 0.04 (1σ; n = 60) (Fig. S3), suggesting aqueous Hg^{2+} photoreduction (Δ^{199}Hg/Δ^{201}Hg ~1.0; Bergquist and Blum, 2007) prior to sedimentation.

Positive Δ^{199}Hg values were observed near the open sea (Fig. 2b). The Hg^{2+} photoreduction results in negative Δ^{199}Hg in the Hg product and positive Δ^{199}Hg in the residue aqueous phase (Bergquist and Blum, 2007; Gratz et al., 2010; Woerndle et al., 2018). Hg^{2+} photoreduction readily occurs in cloud droplets, resulting in positive Δ^{199}Hg values in dissolved Hg^{2+}, which is deposited via precipitation due to its high solubility (Mason and Sheu, 2002). Atmospheric particles and associated pollutants derived from Asian dust are deposited into the ECS in spring and winter annually (Guo et al., 2006), and air masses passing Mainland China have altered Hg isotope composition in the atmospheric samples in the marine boundary layer of the ECS(Fu et al., 2019). Compared to coastal areas, atmospheric deposition is thought to contribute more Hg to the open ocean (Fu et al., 2010; Yin et al., 2015); thus, open sea sediments are characterized by more pronounced positive Δ^{199}Hg values, as has been observed in deep sea sediments in the South China Sea (0.35 ± 0.09‰; 1σ; n = 6) (Yin et al., 2015), San Francisco Bay region (0.17 ± 0.03‰; 1σ; n = 5) (Donovan et al., 2013), Central Portuguese Margin (0.09 ± 0.04‰; 1σ; n = 8) (Mil-Homens et al., 2013), and mid-Pleistocene sapropels from the Mediterranean Sea (0.11 ± 0.03‰; 1σ; n = 5) (Gehrke et al., 2009). Regions far offshore have clearer water and slower sediment accumulation (Chang et al., 2019; Lepak et al., 2018), which may promote Hg^{2+} photoreduction in seawater (Donovan

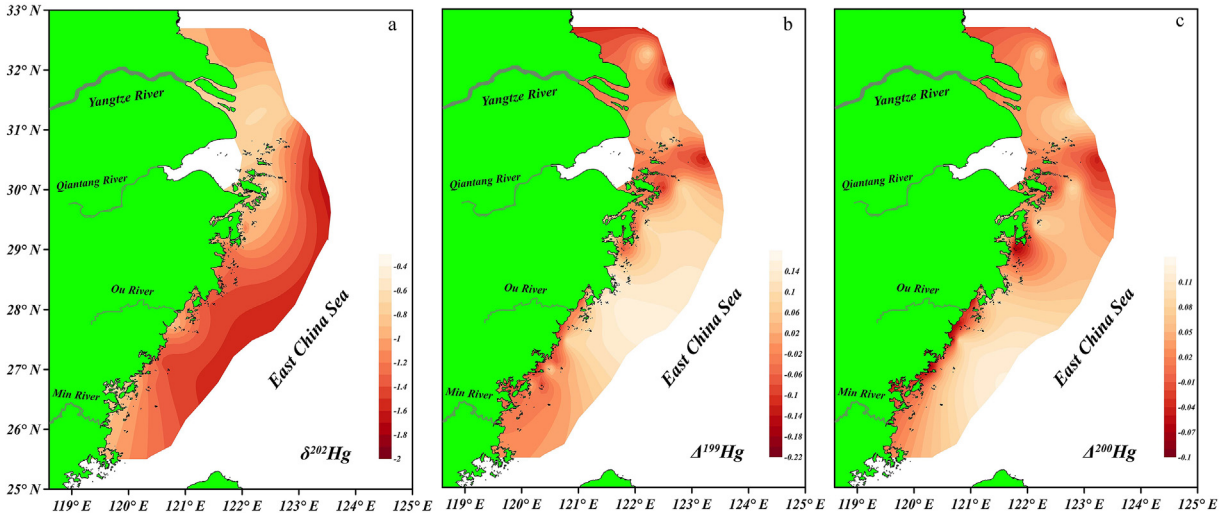

Fig. 2. Distribution of (a) δ^{202}Hg, (b) Δ^{199}Hg, and (c) Δ^{200}Hg in the YRE–ECS inner shelf sediments.

et al., 2013).

Negative Δ^{199}Hg values were observed in coastal sediments and around the YRE islands (Fig. 2b). As a result of Hg^{2+} photoreduction, gaseous Hg (0) species are characterized by negative Δ^{199}Hg values (Yu et al., 2016; Rolison et al., 2013; Gratz et al., 2010; Sherman et al., 2010). Gaseous elemental Hg (0) is readily taken up by vegetation (Demers et al., 2013) and enters the soil through litterfall; therefore, soil Hg is characterized by negative Δ^{199}Hg (Zhang et al., 2013; Wang et al., 2016). Soil particle Hg mainly from the mainland as well as possible islands can be transported to the coastal zone by surface runoff and settle to the bottom sediments (Fitzgerald et al., 2007).

We observed large variation in Δ^{199}Hg (−0.22 to 0.08‰) in YRE sediments (Fig. 2b), indicating sources of sediment Hg apart from surface runoff from the Yangtze River. The Yangtze River flows through the Yangtze River Delta Economic Belt, which is among the most industrialized and urbanized regions of China. Hydrothermal ores, a major source of industrial Hg, are widely used in various industries in China, including battery, paint, light bulb, and explosives production (Yin et al., 2013; Yin et al., 2016a,b,c; Yin et al., 2018). These industrial sources can discharge large amounts of industrial Hg into adjacent aquatic ecosystems. According to previous reports, sediments near known industrial sources present insignificant Hg-MIF and significant Hg-MDF (δ^{202}Hg, −0.53 ± 0.51‰; Δ^{199}Hg, −0.02 ± 0.11‰; 1σ; n = 481) (Bonsignore et al., 2015; Guedron et al., 2016; Wiederhold et al., 2015; Yin et al., 2016a,b,c). The significantly negative δ^{202}Hg values for YRE sediments are characteristic of industrial Hg (Fig. 2a), indicating that the industrial Hg via river discharge is a key source. Therefore, the large variation observed in Δ^{199}Hg values for YRE sediments in the present study could be mainly attributed to the mixing of different sources with distinct Hg isotopic compositions.

Compared with Hg isotopic compositions in sediments from different estuaries/marine regions, those in the Chinese marginal sea presented a clearer and wider range of MDF signatures than those in other areas worldwide (Fig. 3), perhaps due to environmental diversity and the vast industrial system along the long coast of China. Compared with areas having intense human activity such as the YRE, ECS inner shelf, relatively insignificant MIF has been reported for the Pearl River Estuary (Yin et al., 2015), Hackensack River Estuary (Reinfelder and Janssen, 2019), Mediterranean Sea (Gehrke et al., 2009), Consumes River and San Francisco Bay (Gehrke et al., 2011), or in regions distant from intense human

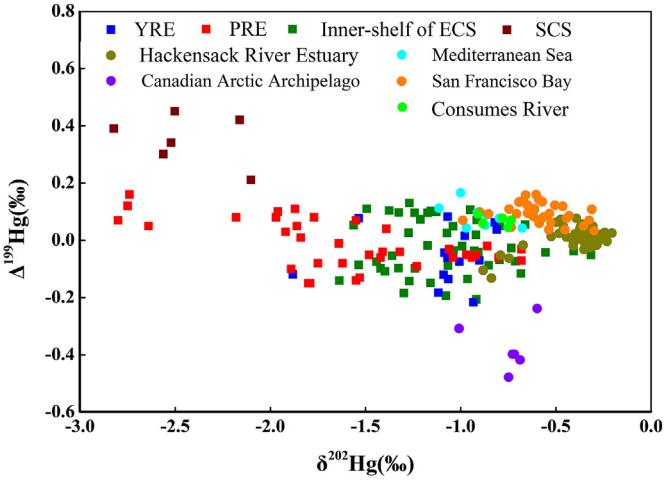

Fig. 3. Sediment mercury (Hg) isotope compositions in estuary/marine areas worldwide (Table S4). PRE: Pearl River Estuary; SCS: South China Sea. Data were derived from previous publications for PRE and SCS (Yin et al., 2015), Mediterranean Sea (Gehrke et al., 2009), San Francisco Bay (Gehrke et al., 2011), Hackensack River Estuary (Reinfelder and Janssen, 2019), and Canadian Arctic Archipelago (Strok et al., 2019).

active areas such as the South China Sea (Yin et al., 2015) and Canadian Arctic Archipelago (Strok et al., 2019). Yin et al. (2015) reported that riverine deliveries of urban and industrial waste are the most important Hg sources in the Pearl River Estuary. Legacy Hg contamination in Berry's Creek, which was polluted by industrially produced liquid Hg, was the dominant Hg source in the Hackensack River Estuary (Reinfelder and Janssen, 2019). Hg mines and/or industrial processes in New Almaden and New Idria were primary Hg sources in San Francisco Bay sediments (Gehrke et al., 2011). These areas, which are all influenced by intensive human activity, presented similar MIF signatures, with industrial Hg as the dominant source. Atmospheric Hg deposition, usually with positive MIF signatures, is the primary source in the open ocean, such as in the South China Sea (Yin et al., 2015). However, atmospheric Hg produced from volcanic and hydrothermal emissions presents an insignificant MIF signature compared with industrial Hg (Fig. 3), which is the largest Hg source in mid-Pleistocene western Mediterranean sediments (Gehrke et al., 2009). Sediments from the Canadian Arctic Archipelago, which is also far from any known

anthropogenic Hg point source emissions, presents a signature opposite that of open ocean sediments in terms of both MDF and MIF (Fig. 3), which could be attributed to atmospheric Hg from coal combustion (Strok et al., 2019). Therefore, distinct Hg sources with different isotopic compositions and Hg isotope fractionation during biogeochemical cycling could explain the wide variation in Hg isotopic composition among regions (Bergquist and Blum, 2007; Blum and Bergquist, 2007; Blum et al., 2014; Yin et al., 2015; Yuan et al., 2019; Zheng et al., 2019).

To evaluate whether the occurrence of Hg isotopic compositions of sediments in the inner shelf of the ECS were primary influenced by the sources of Hg or the sediment resuspension and transportation from the YRE to the south we selected a transect formed by mud area sampling points (E6, E7, E12, E13, E14, E15, E16, S1, S5, S15, S20, S27, S30, S35, S39, and S49) at a depth of about 40 m (Fig. 1). Fig. 4 shows slight variation in Δ^{199}Hg and Δ^{200}Hg. High halide levels in seawater could suppress Hg^{2+} photoreduction due to the formation of stable Hg^{2+} complexes with halides (Whalin et al., 2007); the area near shore had a higher sedimentation rate and lower water clarity, accelerating Hg deposition to surface sediments (Skyllberg et al., 2006) and reducing opportunities for Hg^{2+} exposure to sunlight. Therefore, Hg^{2+} photoreduction MIFs were limited, and the slight variation in Δ^{199}Hg and Δ^{200}Hg could be attributed to Hg source signatures in the near shore area. δ^{202}Hg and Δ^{199}Hg values showed similar trends along the transect, remaining relatively stable at the YRE, decreasing in the inner shelf area, and then fluctuating as they increased to higher levels in the Min River Estuary (Fig. 4). In the YRE area (E6-E16), features of Hg isotopic composition were consistent with those of industrial Hg sources, indicating large impacts on Hg isotopic composition by industrial Hg discharge into rivers. The lower stage (S1–S15) near the coastal area was affected mainly by soil Hg via surface runoff; the rising stage (S20, S27) was influenced by the Ou River, which also transports large amounts of industrial Hg to the coastal sea. The fluctuating increase stage (S30–S39) was influenced by local rivers like the Feiyun River, and the S49 sampling point showed a clear MDF and insignificant MIF, which may be attributed to the great influence of a large industrial pollution point source for the Min River. These results suggest that the regional large rivers could have a great influence on Hg isotopic compositions in the inner shelf, whereas the impact of resuspension and transportation processes on Hg isotopic compositions should be very limited. This is likely due to that the fine-grained sediments usually contain a high content of organic matter (e.g., humic acid, fulvic acid, and amino acids) in the estuarine-inner shelf system, which has a strong affinity to bind with Hg (Berto et al., 2006; Ramalhosa et al., 2006; Skyllberg et al., 2006).

3.2. Quantitative source discrimination of Hg

As described above, the sediment Hg isotopic composition can mainly reflect the mixing of Hg from distinct sources with different isotopic compositions. An isotope-based triple-mixing model has been widely and successfully applied to apportion Hg sources in Chinese marginal sea sediments (Liu et al., 2011; Zhang et al., 2018; Yin et al., 2018; Meng et al., 2019), including three Hg sources: industrial activity, soil, and precipitation. As shown in Fig. 5, samples from the YRE and inner shelf showed similar admixtures in Hg isotopic composition (*t*-test, $p < 0.05$), and almost all sampling points in this study were within the triangle created by the three sources, predicting a close match between the Hg sources of these samples and the three potential sources included in the model.

To further quantify the contributions of industrial Hg, soil Hg,

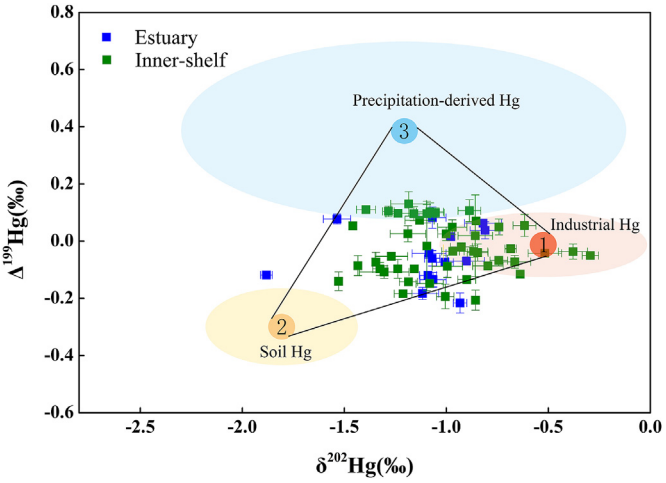

Fig. 5. Triple-mixing model of industrial Hg discharged into river water, soil Hg, and precipitation-derived atmospheric deposition Hg in sediments from the YRE–ECS inner shelf. Red area represents industrial Hg (δ^{202}Hg, −0.53 ± 0.51‰; Δ^{199}Hg, −0.02 ± 0.11‰; 1σ; n = 481), as estimated by Hg polluted sediments near known industrial sources (Bonsignore et al., 2015; Guedron et al., 2016; Wiederhold et al., 2015; Yin et al., 2016a,b,c). Yellow area represents soil Hg (δ^{202}Hg, −1.82 ± 0.39‰; Δ^{199}Hg, −0.29 ± 0.12‰; 1σ; n = 156). Blue area represents precipitation-derived Hg (δ^{202}Hg, −1.22 ± 1.08‰; Δ^{199}Hg, 0.38 ± 0.33‰; 1σ; n = 117) (Yin et al., 2018). (For interpretation of the references to colour in this figure legend, the reader is referred to the Web version of this article.)

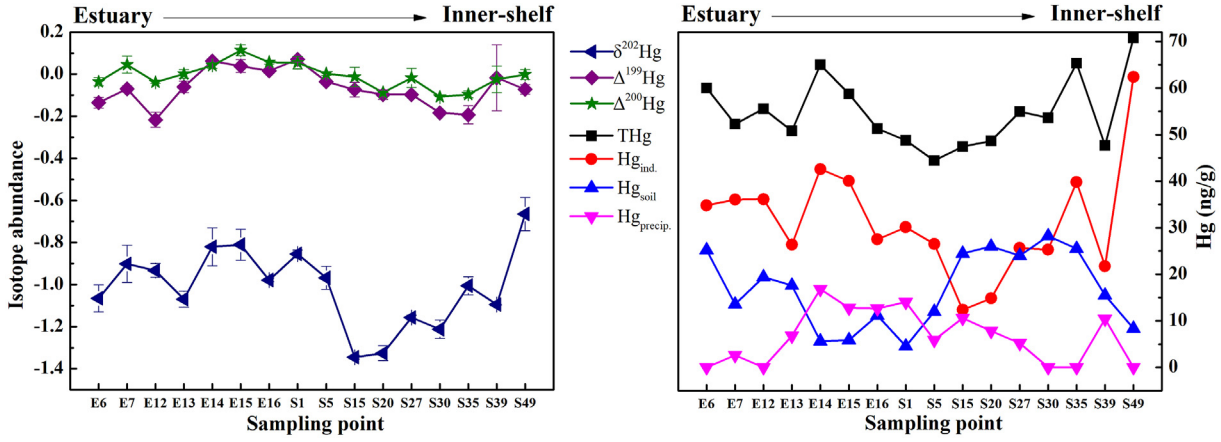

Fig. 4. Distribution of Hg isotopic compositions and concentrations in mud area sampling sites from north to south in the study area.

and precipitation-derived Hg, the triple-mixing model was used as follows:

$$\begin{aligned}\Delta^{199}\mathrm{Hg}_{\mathrm{sample}} &= \mathrm{Find.}\cdot\Delta^{199}\mathrm{Hg}_{\mathrm{ind.}} + \mathrm{Fsoil}\cdot\Delta^{199}\mathrm{Hg}_{\mathrm{soil}} + \mathrm{Fprecip.}\cdot\Delta^{199}Hg_{\mathrm{precip.}}\\ \delta^{202}\mathrm{Hg}_{\mathrm{sample}} &= \mathrm{Find.}\cdot\delta^{202}\mathrm{Hg}_{\mathrm{ind.}} + \mathrm{Fsoil}\cdot\delta^{202}Hg_{\mathrm{soil}} + \mathrm{Fprecip.}\cdot\delta^{202}Hg_{\mathrm{precip.}}\\ \mathrm{Find.} + \mathrm{Fsoil} + \mathrm{Fprecip.} &= 1\end{aligned} \quad (3)$$

where F_{ind}, F_{soil}, and F_{precip} are the fractions of industrial, soil, and precipitation Hg, respectively; $\delta^{202}Hg_{ind}$, $\delta^{202}Hg_{soil}$, and $\delta^{202}Hg_{precip}$ are the $\delta^{202}Hg$ of industrial, soil, and precipitation Hg, respectively; and $\Delta^{199}Hg_{ind}$, $\Delta^{199}Hg_{soil}$, and $\Delta^{199}Hg_{precip}$ are the $\Delta^{199}Hg$ of industrial, soil, and precipitation Hg, respectively. We adjusted negative F values to zero, redistributed the weights, and ensured that $F_{ind} + F_{soil} + F_{precip} = 1$.

The model results are shown in Table S5. The major contribution was from industrial Hg (F_{ind}, mean, 51.8 ± 24.5%; 1σ; n = 60), followed by soil Hg (F_{soil}, mean, 29.2 ± 17.0%; 1σ; n = 60) and precipitation Hg (F_{precip}, mean, 19.1 ± 17.5%; 1σ; n = 60). The concentrations of industrial Hg (Hg_{ind}), soil Hg (Hg_{soil}), and precipitation Hg (Hg_{precip}) were calculated as follows:

$$\begin{aligned}\mathrm{Hg}_{ind.} &= F_{ind.}\cdot Hg_{sample}\\ \mathrm{Hg}_{soil} &= F_{soil}\cdot Hg_{sample}\\ Hg_{precip.} &= F_{precip.}\cdot Hg_{sample}.\end{aligned} \quad (4)$$

As shown in Fig. 6, the concentration of industrial Hg (0–91.9 ng g^{-1}, mean 28.9 ± 18.4 ng g^{-1}) tended to decrease as offshore distance increased, similar to the trend in total Hg distribution in the sediments, suggesting that Hg occurrence was mainly controlled by industrial Hg, which accounted for 77.4% of the variance in total Hg (Fig. S4). The concentration of industrial Hg discharged into water at the YRE was significantly higher than that in other regions, indicating that Yangtze River discharge is a key process impacting Hg levels in sediments of this marginal sea. Precipitation-derived Hg (0–30.0 ng g^{-1}, mean 8.73 ± 7.92 ng g^{-1}) in the offshore area near the open sea was significantly higher than that in other areas, perhaps due to the higher contribution of precipitation-derived atmospheric Hg deposition in the open sea. Soil Hg concentrations (0–28.4 ng g^{-1}, mean 13.8 ± 7.22 ng g^{-1}) were higher in the ECS inner shelf than in the YRE, likely due to surface runoff and soil-derived Hg concentrations also were higher around islands of the YRE, further suggesting that the island soil could be a potential source for Hg in the region.

3.3. Depositional fluxes and inventory of three major Hg sources

Considering that sediment Hg may be diluted or concentrated by inputs from mineral and organic matter, Hg depositional fluxes better indicators of Hg inputs than Hg concentrations alone. Therefore, Hg depositional fluxes (ng cm^{-2} yr^{-1}) of industrially derived Hg discharged into water, soil Hg via surface runoff, and precipitation-derived atmospheric deposition Hg were estimated based on the following formula:

$$\mathrm{Fluxi} = \mathrm{Ci}\cdot\rho\cdot\mathrm{pi}, \quad (5)$$

where Ci is the Hg concentration at sample site i (ng g^{-1}). The dry density (ρ) is assumed to 1.2 g cm^{-3}, which is a recommended data of marine sediment dry density by Liu et al. (2007) in the ECS, and pi is the sedimentation rate at each sample site (Huh and Su, 1999; Liu et al., 2006). The depositional fluxes of THg in YRE-ECS inner shelf sediments ranged from 15.0 to 120 ng cm^{-2} yr^{-1} (61.9 ± 31.4 ng cm^{-2} yr^{-1}, 1σ, n = 60). Industrially derived Hg depositional fluxes (0–118 ng cm^{-2} yr^{-1}; 35.0 ± 27.3 ng cm^{-2} yr^{-1}, 1σ, n = 60) were followed by soil-derived Hg depositional fluxes (0–50.86 ng cm^{-2} yr^{-1}; 16.5 ± 12.9 ng cm^{-2} yr^{-1}, 1σ, n = 60) and precipitation-derived atmospheric deposition Hg (0–42.62 ng cm^{-2} yr^{-1}; 10.5 ± 11.1 ng cm^{-2} yr^{-1}, 1σ, n = 60). The spatial distribution characteristics of depositional fluxes of THg, industrial Hg via discharge into water, soil Hg via surface runoff, and precipitation-derived atmospheric deposition Hg in YRE-ECS inner shelf sediments (Fig. 7) were similar to the distribution patterns of Hg concentration derived from the three sources. This suggests that the Hg source was the major factor for the Hg isotopic compositions; while the effect of in-situ phase transformation and hydrodynamic alteration could be a second one in the region. The sampling sites divided the study area into compartments, each with a sampling site at the center. We assumed that Hg concentrations from different sources in each compartment were homogeneous and equal to the corresponding sample site concentration to estimate a mass inventory (I, t yr^{-1}) according to depositional fluxes and compartment areas (Lin et al., 2013; Liu et al., 2017). Detailed information about each compartment mass inventory is provided in Table S6; the total mass inventory of industrial Hg via discharge into water was 25.6 t yr^{-1}, followed by a soil-derived Hg mass inventory of 13.0 t yr^{-1} and precipitation-derived atmospheric deposition Hg mass inventory of 7.56 t yr^{-1}. Generally, depositional fluxes and mass inventories were about 2-fold higher for industrial Hg than for soil Hg and >3-fold higher than for precipitation Hg. Thus, industrial Hg had the highest mean depositional fluxes and mass inventory, accounting for 77.4% of the total variance in Hg in the YRE and ECS inner shelf.

4. Conclusion

In this study, we combined an Hg isotope source apportionment approach with Hg deposition fluxes and confirmed that industrial Hg discharged into rivers, soil Hg via surface runoff, and precipitation-derived atmospheric deposition Hg were the major Hg contributors in YRE-ECS inner shelf sediments. Industrial Hg discharged into water accounted for 77.4% of the total variance in Hg, with the highest mean deposition flux (35.0 ± 27.3 ng cm^{-2} yr^{-1}) and mass inventory (25.6 t yr^{-1}). Soil Hg via surface runoff and precipitation-derived atmospheric Hg had mean deposition fluxes of 16.5 ± 12.9 and 10.5 ± 11.1 ng cm^{-2} yr^{-1}, respectively. Soil Hg via surface runoff was significant in coastal areas, whereas precipitation-derived atmospheric Hg had a greater influence in offshore regions. Variation in Hg isotopic compositions along the coastal area from north to south was mainly attributed to large regional riverine inputs rather than sediment resuspension and transportation processes. The large river estuary and adjacent shelf play key roles in the regional Hg biogeochemical cycling. This study provides evidence that isotopic Hg composition can serve as a robust tracer of Hg sources in sediments in complex dynamic

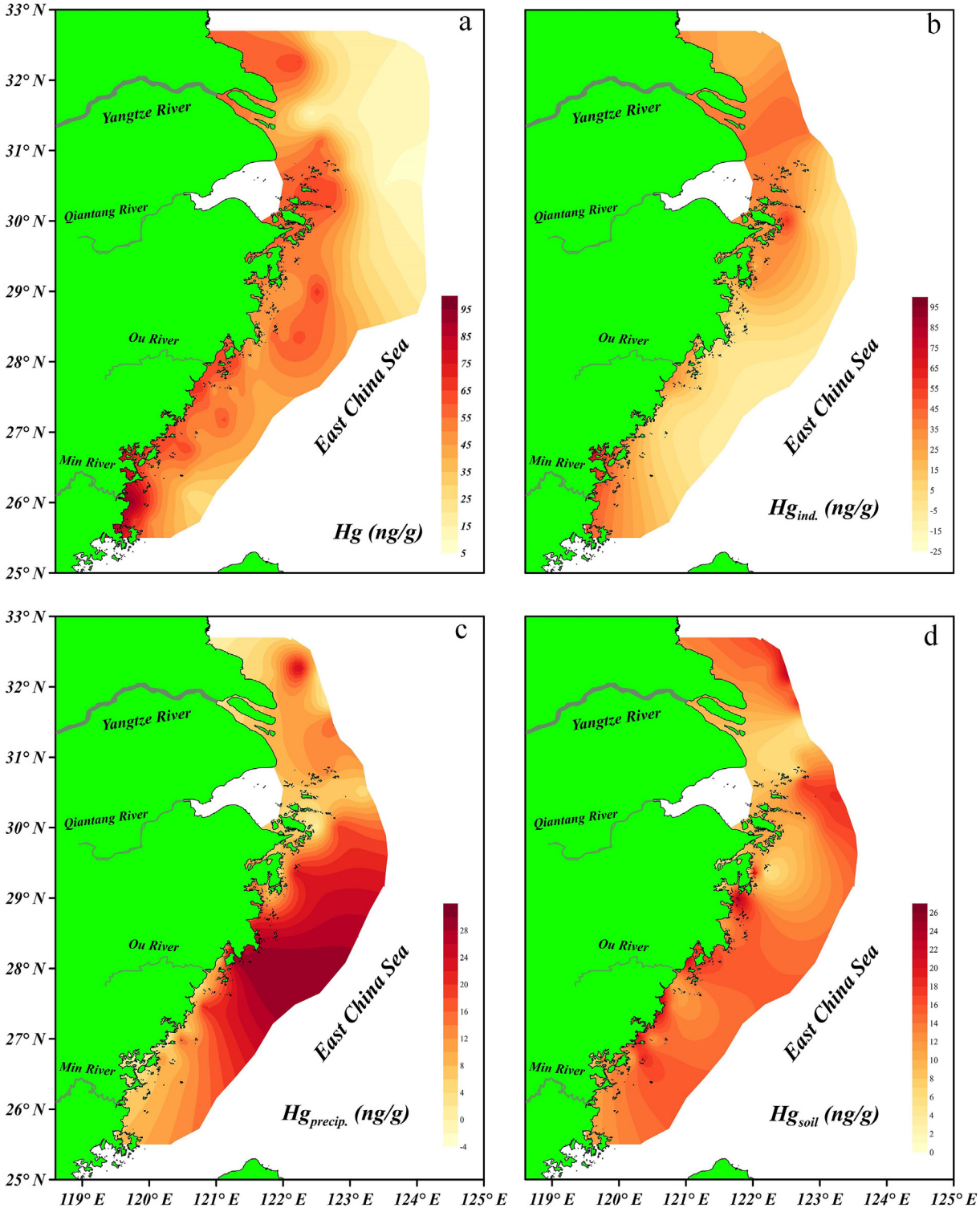

Fig. 6. Distribution of (a) THg, (b) industrial Hg discharged into water, (c) soil Hg via surface runoff, and (d) precipitation-derived atmospheric deposition Hg in YRE–ECS inner shelf sediments.

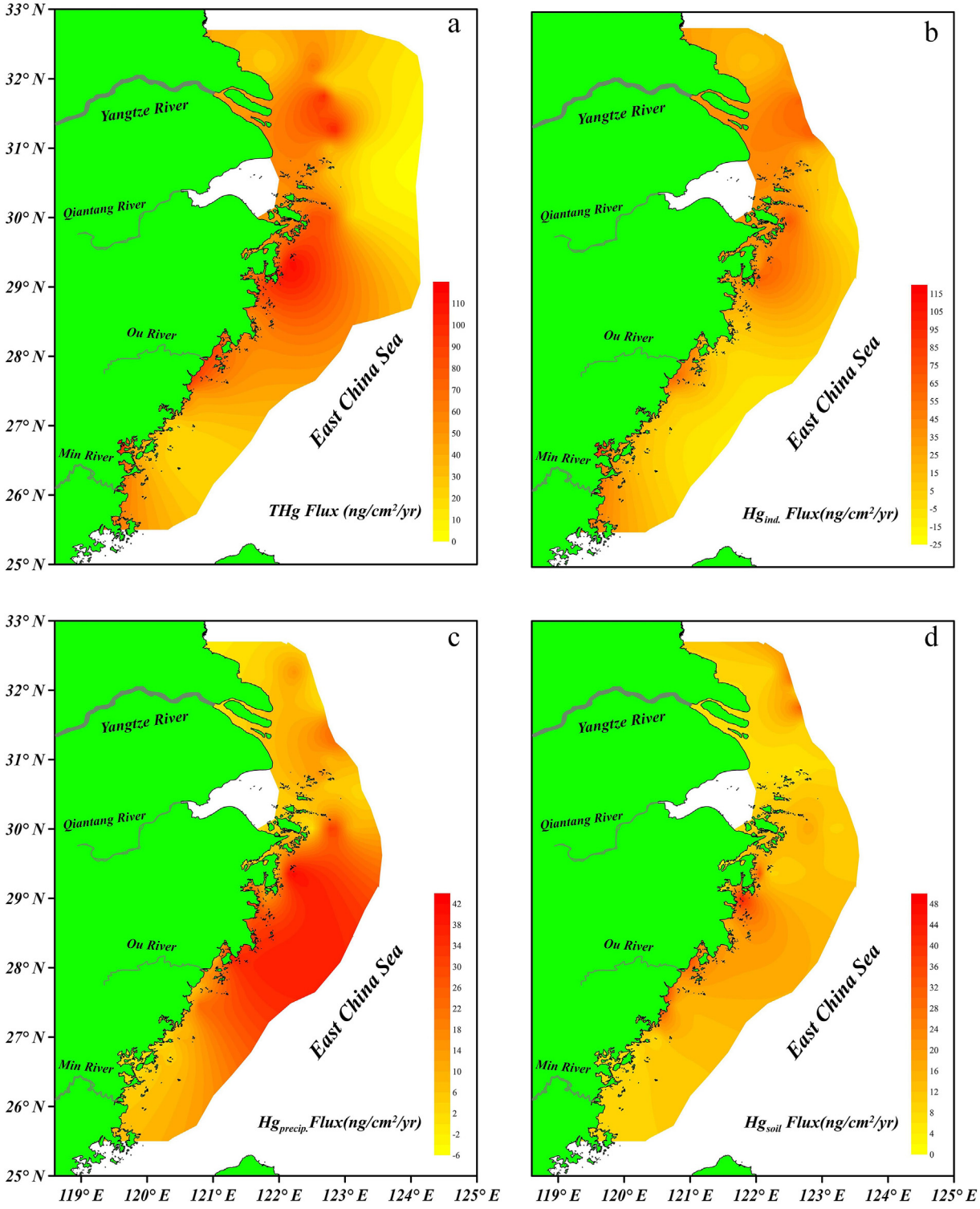

Fig. 7. Distribution of deposition fluxes of (a) THg, (b) industrial Hg via discharge into water, (c) soil Hg via surface run-off, and (d) precipitation-derived atmospheric deposition Hg in YRE–ECS inner shelf sediments.

estuarine–inner shelf domains.

Declaration of competing interest

The authors declare that they have no known competing financial interests or personal relationships that could have appeared to influence the work reported in this paper.

CRediT authorship contribution statement

Xiang Sun: Writing - original draft, Formal analysis, Software, Visualization, Data curation, Validation. **Runsheng Yin:**

Methodology, Data curation, Writing - review & editing. **Limin Hu:** Investigation, Resources, Writing - review & editing. **Zhigang Guo:** Project administration, Resources, Conceptualization, Writing - review & editing, Supervision. **James P. Hurley:** Writing - review & editing, Investigation. **Ryan F. Lepak:** Investigation. **Xiangdong Li:** Writing - review & editing.

Acknowledgments

This work was supported by the National Natural Science Foundation of China (NSFC) (Nos.: 41722603 and 41676034) and the Basic Scientific Fund for National Public Research Institutes of China (2017S01). The reviewers should be sincerely appreciated for their constructive comments that greatly improved this paper.

Appendix A. Supplementary data

Supplementary data to this article can be found online at https://doi.org/10.1016/j.envpol.2020.114356.

References

Bergquist, B.A., Blum, J.D., 2007. Mass-dependent and -independent fractionation of Hg isotopes by photoreduction in aquatic systems. Science 318 (5849), 417–420.
Berto, D., Giani, M., Covelli, S., Bosc, R., Cornello, M., Macchia, S., Massironi, M., 2006. Mercury in sediments and Nassarius reticulatus (gastropoda, prosobranchia) in the southern Venice lagon. Sci. Total Environ. 368, 298–305.
Bianchi, T.S., Allison, M.A., 2009. Large-river delta-front estuaries as natural "recorders" of global environmental change. Proc. Natl. Acad. Sci. U.S.A. 106 (20), 8085–8092.
Blum, J.D., Bergquist, B.A., 2007. Reporting of variations in the natural isotopic composition of mercury. Anal. Bioanal. Chem. 388 (2), 353–359.
Blum, J.D., Sherman, L.S., Johnson, M.W., 2014. Mercury isotopes in earth and environmental sciences. In: Jeanloz, R., Jeanloz, R., Jeanlozs, R., | (Eds.), Annual Review of Earth and Planetary Sciences, pp. 249–269.
Bonsignore, M., Tamburrino, S., Oliveri, E., Marchetti, A., Durante, C., Berni, A., Quinci, E., Sprovieri, M., 2015. Tracing mercury pathways in Augusta Bay (southern Italy) by total concentration and isotope determination. Environ. Pollut. 205, 178–185.
Buchachenko, A.L., Lukzen, N.N., Pedersen, J.B., 2007. On the magnetic field and isotope effects in enzymatic phosphorylation. Chem. Phys. Lett. 434 (1–3), 139–143.
Chang, L., Tang, H., Yi, S., Sun, W.K., 2019. The trend and seasonal change of sediment in the East China Sea detected by GRACE. Geophys. Res. Lett. 46 (3), 1250–1258.
Demers, J.D., Blum, J.D., Zak, D.R., 2013. Mercury isotopes in a forested ecosystem: implications for air-surface exchange dynamics and the global mercury cycle. Global Biogeochem. Cycles 27, 222–238.
Donovan, P.M., Blum, J.D., Yee, D., Gehrke, G.E., Singer, M.B., 2013. An isotopic record of mercury in San Francisco Bay sediment. Chem. Geol. 349, 87–98.
Driscoll, C.T., Mason, R.P., Chan, H.M., Jacob, D.J., Pirrone, N., 2013. Mercury as a global pollutant: sources, pathways, and effects. Environ. Sci. Technol. 47 (10), 4967–4983.
Du, J., Zhao, J., Chen, B., Chen, M., Zhou, T., Ma, Z., Yu, Y., Hu, W., 2013. Assessing ecological risks of heavy metals to marine organisms in Chinese offshore and Fujian main bays by species sensitivity distributions. Asian J. Ecotoxicol. 4, 554–560 (in Chinese with English abstract).
Estrade, N., Carignan, J., Sonke, J.E., Donard, O.F.X., 2009. Mercury isotope fractionation during liquid-vapor evaporation experiments. Geochem. Cosmochim. Acta 73 (10), 2693–2711.
Fitzgerald, W.F., Lamborg, C.H., Hammerschmidt, C.R., 2007. Marine biogeochemical cycling of mercury. Chem. Rev. 107 (2), 641–662.
Fu, X.W., Feng, X.B., Zhang, G., Xu, W.H., Li, X.D., Yao, H., Liang, P., Li, J., Sommar, J., Yin, R.S., Liu, N., 2010. Mercury in the marine boundary layer and seawater of the South China Sea: concentrations, sea/air flux, and implication for land outflow. J. Geophys. Res. Atmos. 115 (D06303).
Fu, X.W., Zhang, H., Feng, X.B., Tan, Q.Y., Ming, L.L., Liu, C., Zhang, L.M., 2019. Domestic and transboundary sources of atmospheric particulate bound mercury in remote areas of China: evidence from mercury isotopes. Environ. Sci. Technol. 53 (4), 1947–1957.
Gehrke, G.E., Blum, J.D., Meyers, P.A., 2009. The geochemical behavior and isotopic composition of Hg in a mid-Pleistocene western Mediterranean sapropel. Geochem. Cosmochim. Acta 73 (6), 1651–1665.
Gehrke, G.E., Blum, J.D., Marvin-DiPasquale, M., 2011. Source of mercury to Francisco Bay surface sediment as revealed by mercury stable isotopes. Geochem. Cosmochim. Acta 75 (3), 691–705.
Ghosh, S., Schauble, E.A., Couloume, G.L., Blum, J.D., Bergquist, B.A., 2013. Estimation of nuclear volume dependent fractionation of mercury isotopes in equilibrium liquid-vapor evaporation experiments. Chem. Geol. 336 (SI), 5–12.
Gratz, L.E., Keeler, G.J., Blum, J.D., Sherman, L.S., 2010. Isotopic composition and fractionation of mercury in Great Lakes precipitation and ambient air. Environ. Sci. Technol. 44 (20), 7764–7770.
Guedron, S., Amouroux, D., Sabatier, P., Desplanquee, C., Develle, A.L., Barre, J., Feng, C., Guiter, F., Arnaud, F., Reyss, J.L., Charlet, L., 2016. A hundred year record of industrial and urban development in French Alps combining Hg accumulation rates and isotope composition in sediment archives from Lake Luitel. Chem. Geol. 431, 10–19.
Guo, Z.G., Lin, T., Zhang, G., Zheng, M., Zhang, Z.Y., Hao, Y.C., Fang, M., 2007. The sedimentary fluxes of polycyclic aromatic hydrocarbons in the Yangtze River Estuary coastal sea for the past century. Sci. Total Environ. 386 (1–3), 33–41.
Guo, Z.G., Lin, T., Zhang, G., Yang, Z., Fang, M., 2006. High-resolution depositional records of polycyclic aromatic hydrocarbons in the central continental shelf mud of the East China Sea. Environ. Sci. Technol. 40 (17), 5304–5311.
Huh, C.A., Su, C.C., 1999. Sedimentation dynamics in the east China sea elucidated from Pb-210, Cs-137 and Pu-239, Pu-240. Mar. Geol. 160 (1–2), 183–196.
Lepak, R.F., Janssen, S.E., Yin, R.S., Krabbenhoft, D.P., Ogorek, J.M., DeWild, J.F., Tate, M.T., Holsen, T.M., Hurley, J.P., 2018. Factors affecting mercury stable isotopic distribution in piscivorous fish of the Laurentian Great Lakes. Environ. Sci. Technol. 52 (5), 2768–2776.
Li, Z.X., Lin, T., Li, Y.Y., Jiang, Y.Q., Guo, Z.G., 2017. Atmospheric deposition and air-sea gas exchange fluxes of DDT and HCH in the Yangtze River estuary, east China sea. J. Geophys. Res.: Atmos. 122 (14), 7664–7677.
Lin, T., Hu, L.M., Guo, Z.G., Zhang, G., Yang, Z., 2013. Deposition fluxes and fate of polycyclic aromatic hydrocarbons in the Yangtze River estuarine-inner shelf in the East China Sea. Global Biogeochem. Cycles 27 (1), 77–87.
Liu, J.L., Feng, X.B., Yin, R.S., Zhu, W., Li, Z.G., 2011. Mercury distributions and mercury isotope signatures in sediments of Dongjiang, the Pearl River Delta, China. Chem. Geol. 287 (1–2), 81–89.
Liu, J.P., Li, A.C., Xu, K.H., Veiozzi, D.M., Yang, Z.S., Milliman, J.D., DeMaster, D., 2006. Sedimentary features of the Yangtze River-derived along-shelf clinoform deposit in the east China sea. Continent. Shelf Res. 26 (17–18), 2141–2156.
Liu, J.P., Xu, K.H., Li, A.C., Milliman, J.D., Velozzi, D.M., Xiao, S.B., Yang, Z.S., 2007. Flux and fate of Yangtze River sediment delivered to the east China sea. Geomorphology 85 (3–4), 208–224.
Liu, M.D., Chen, L., Wang, X.J., Zhang, W., Tong, Y.D., Ou, L.B., Xie, H., Shen, H.Z., Ye, X.J., Deng, C.Y., Wang, H.H., 2016. Mercury export from mainland China to adjacent seas and its influence on the marine mercury balance. Environ. Sci. Technol. 50 (12), 6224–6232.
Liu, W.C., Hu, L.M., Lin, T., Li, Y.Y., Guo, Z.G., 2017. Distribution and mass inventory of mercury in sediment from the Yangtze River estuarine-inner shelf of the East China Sea. Continent. Shelf Res. 132, 29–37.
Mahaffey, K.R., Sunderland, E.M., Chan, H.M., Choi, A.L., Grandjean, P., Marien, K., Oken, E., Sakamoto, M., Schoeny, R., Weihe, P., Yan, C.H., Yasutake, A., 2011. Balancing the benefits of n-3 polyunsaturated fatty acids and the risks of methylmercury exposure from fish consumption. Nutr. Rev. 69 (9), 493–508.
Martinez-Cortizas, A., Pontevedra-Pombal, X., Garcia-Rodeja, E., Novoa-Munoz, J.C., Shotyk, W., 1999. Mercury in a Spanish peat bog: archive of climate change and atmospheric metal deposition[J]. Science 284 (5416), 939–942.
Mason, R.P., Sheu, G.R., 2002. Role of the ocean in the global mercury cycle. Global Biogeochem. Cycles 16, 10934.
Meng, M., Sun, R.Y., Liu, H.W., Yu, B., Yin, Y.G., Hu, L.G., Shi, J.B., Jiang, G.B., 2019. An integrated model for input and migration of mercury in Chinese coastal sediments. Environ. Sci. Technol. 53 (5), 2460–2471.
Mil-Homens, M., Blum, J.D., Canario, J., Caetano, M., Costa, A.M., Lebreiro, S.M., Trancoso, M., Richter, T., de Stigter, H., Johnson, M., Branco, V., Cesario, R., Mouro, F., Mateus, M., Boer, W., Melo, Z., 2013. Tracing anthropogenic Hg and Pb input using stable Hg and Pb isotope ratios in sediments of the central Portuguese Margin. Chem. Geol. 336 (SI), 62–71.
Milliman, J.D., Beardsley, R.C., Yang, Z.S., Limeburner, R., 1985. Modern Huanghe-derived muds on the outer shelf of the East China Sea - identification and potential transport mechanisms. Continent. Shelf Res. 4 (1–2), 175–188.
Outridge, P.M., Mason, R.P., Wang, F., Guerrero, S., Heimbürger-Boavida, L.E., 2018. Updated global and oceanic mercury budgets for the United Nations global mercury assessment 2018. Environ. Sci. Technol. 52 (20), 11466–11477.
Ramalhosa, E., Pato, P., Montreeoso, P., Pereira, E., Vale, E., Duarte, A.C., 2006. Accumilation versus remobilization of mercury in sediments of a contaminated lagoon. Mar. Pollut. Bull. 52, 332–356.
Reinfelder, J.R., Janssen, S.E., 2019. Tracking legacy mercury in the Hackensack River estuary using mercury stable isotopes. J. Hazard Mater. 375, 121–129.
Rolison, J.M., Landing, W.M., Luke, W., Cohen, M., Salters, V.J.M., 2013. Isotopic composition of species-specific atmospheric Hg in a coastal environment. Chem. Geol. 336 (SI), 37–49.
Schauble, E.A., 2007. Role of nuclear volume in driving equilibrium stable isotope fractionation of mercury, thallium, and other very heavy elements. Geochem. Cosmochim. Acta 71 (9), 2170–2189.
Sherman, L.S., Blum, J.D., Johnson, K.P., Keeler, G.J., Barres, J.A., Douglas, T.A., 2010. Mass-independent fractionation of mercury isotopes in Arctic snow driven by sunlight. Nat. Geosci. 3 (3), 173–177.
Skyllberg, U., Bloom, P.R., Qian, J., Lin, C.M., Bleam, W.F., 2006. Complexation of mercury(II) in soil organic matter: EXAFS evidence for linear two-coordination with reduced sulfur groups. Environ. Sci. Technol. 40 (13), 4174–4180.
Strok, M., Baya, P.A., Dietrich, D., 2019. Mercury speciation and mercury stable isotope composition in sediments from the Canadian Arctic Archipelago. Sci.

Total Environ. 617, 655–665.
Sun, R.Y., Jiskra, Martin Amos, Helen, M., Zhang, Y.X., Sunderland, Elsie M., Sonke, Jeroen E., 2019. Modelling the mercury stable isotope distribution of Earth surface reservoirs: implications for global Hg cycling. Geochem. Cosmochim. Acta 246, 156–173.
Su, S., Zhi, J., Lou, L., Huang, F., Chen, X., Wu, J., 2011. Spatio-temporal patterns and source apportionment of pollution in Qiantang River (China) using neural-based modeling and multivariate statistical techniques. Phys. Chem. Earth, Parts A/B/C 36 (9), 379–386.
Wang, C., Ci, Z., Wang, Z., Zhang, X., 2016. Air-sea exchange of gaseous mercury in the East China Sea. Environ. Pollut. 212, 535–543.
Wang, H.J., Saito, Y., Zhang, Y., Bi, N.S., Sun, X.X., Yang, Z.S., 2011. Recent changes of sediment flux to the western Pacific Ocean from major rivers in East and Southeast Asia. Earth Sci. Rev. 108 (1–2), 80–100.
Whalin, L., Kim, E., Mason, R., 2007. Factors influencing the oxidation, reduction, methylation and demethylation of mercury species in coastal waters. Mar. Chem. 107 (3SI), 278–294.
Wiederhold, J.G., Cramer, C.J., Daniel, K., Infante, I., Bourdon, B., Kretzschmar, R., 2010. Equilibrium mercury isotope fractionation between dissolved Hg(II) species and thiol-Bound Hg. Environ. Sci. Technol. 44 (11), 4191–4197.
Wiederhold, J.G., Skyllberg, U., Drott, A., Jiskra, M., Jonsson, S., Bjorn, E., Bourdon, B., Kretzschmar, R., 2015. Mercury isotope signatures in contaminated sediments as a tracer for local industrial pollution sources. Environ. Sci. Technol. 49 (1), 177–185.
Woerndle, G.E., Tsui, M.T., Sebestyen, S.D., Blum, J.D., Nie, X.P., Kolka, R.K., 2018. New insights on ecosystem mercury cycling revealed by stable isotopes of mercury in water flowing from a headwater peatland catchment. Environ. Sci. Technol. 52 (4), 1854–1861.
Yang, H., Yang, S., Xu, K., Milliman, J.D., Wang, H., Yang, Z., Chen, Z., Zhang, C., 2018. Human impacts on sediment in the Yangtze River: a review and perspectives. Global Planet. Change 162, 8–17.
Yang, S., Li, M., Dai, S., Liu, Z., Zhang, J., Ding, P., 2006a. Drastic decrease in sediment supply from Yangtze River and it challenge to coastal wetland management. Geophys. Res. Lett. 33, L06408.
Yang, Z., Wang, H., Saito, Y., Milliman, J.D., Xu, K., Qiao, S., Shi, G., 2006b. Dam impacts on the Changjiang (Yangtze) River sediment discharge to the sea: the past 55 years and after the Three Gorges Dam. Water Resour. Res. 42 (W044074).
Yin, R.S., Feng, X.B., Wang, J.X., Li, P., Liu, J.L., Zhang, Y., Chen, J.B., Zheng, L., Hu, T.D., 2013. Mercury speciation and mercury isotope fractionation during ore roasting process and their implication to source identification of downstream sediment in the Wanshan mercury mining area, SW China. Chem. Geol. 336 (SI), 72–79.
Yin, R.S., Feng, X.B., Chen, B.W., Zhang, J.J., Wang, W.X., Li, X.D., 2015. Identifying the sources and processes of mercury in subtropical estuarine and ocean sediments using Hg isotopic composition. Environ. Sci. Technol. 49 (3), 1347–1355.
Yin, R.S., Krabbenhoft, D.P., Bergquist, B.A., Zheng, W., Lepak, R.F., Hurley, J.P., 2016a. Effects of mercury and thallium concentrations on high precision determination of mercury isotopic composition by Neptune Plus multiple collector inductively coupled plasma mass spectrometry. J. Anal. At. Spectrom. 31 (10), 2060–2068.
Yin, R.S., Feng, X.B., Hurley, J.P., Krabbenhoft, D.P., Lepak, R.F., Hu, R.Z., Zhang, Q., Li, Z.G., Bi, X.W., 2016b. Mercury isotopes as proxies to identify sources and environmental impacts of mercury in sphalerites. Sci. Rep. 6 (18686).
Yin, R.S., Guo, Z.G., Hu, L.M., Liu, W.C., Hurley, J.P., Lepak, R.F., Lin, T., Feng, X.B., Li, X.D., 2018. Mercury inputs to Chinese marginal seas: impact of industrialization and development of China. J. Geophys. Res.: Oceans 123 (8), 5599–5611.
Yin, R., Lepak, R.F., Krabbenhoft, D.P., Hurley, J.P., 2016c. Sedimentary records of mercury stable isotopes in Lake Michigan. Elementa Sci. Anthropocene 4, 000086.
Yu, B., Fu, X.W., Yin, R.S., Zhang, H., Wang, X., Lin, C.J., Wu, C.S., Zhang, Y.P., He, N.N., Fu, P.Q., Wang, Z.F., Shang, L.H., Sommar, J., Sonke, J.E., Maurice, L., Guinot, B., Feng, X.B., 2016. Isotopic composition of atmospheric mercury in China: New evidence for sources and transformation processes in air and in vegetation. Environ. Sci. Technol. 50 (17), 9262–9269.
Yuan, W., Sommar, J., Lin, C.J., Wang, X., Li, K., Liu, Y., Zhang, H., Lu, Z.Y., Wu, C.S., Feng, X.B., 2019. Stable isotope evidence shows re-emission of elemental mercury vapor occurring after reductive loss from foliage. Environ. Sci. Technol. 53 (2), 651–660.
Zhang, H., Yin, R., Feng, X., Sommar, J., Anderson, C.W.N., Sapkota, A., 2013. Atmospheric mercury inputs in montane soils increase with elevation: evidence from mercury isotope signatures. Sci. Rep. 3, 3322.
Zhang, R., Russell, J., Xiao, X., Zhang, F., Li, T.G., Liu, Z.Y., Guan, M.L., Han, Q., Shen, L.Y., Shu, Y.J., 2018. Historical records, distributions and sources of mercury and zinc in sediments of East China Sea: implication from stable isotopic compositions. Chemosphere 205, 698–708.
Zheng, W., Demers, J.D., Lu, X., Bergquist, B.A., Anbar, A.D., Blum, J.D., Gu, B., 2019. Mercury stable isotope fractionation during abiotic dark oxidation in the presence of thiols and natural organic matter. Environ. Sci. Technol. 53 (4), 1853–1862.
Zheng, W., Hintelmann, H., 2009. Mercury isotope fractionation during photoreduction in natural water is controlled by its Hg/DOC ratio. Geochem. Cosmochim. Acta 73 (22), 6704–6715.
Zheng, W., Hintelmann, H., 2010. Isotope fractionation of mercury during its photochemical reduction by low-molecular-weight organic compounds. J. Phys. Chem. A 114 (12), 4246–4253.